Title

Effect of wavefunction delocalization on shift current generation.

Journal

Journal of Physics Condensed Matter, 31(8)

ISSN

0953-8984

Authors

Tan, Liang Z

Rappe, Andrew M

Publication Date

2019-02-27

DOI

10.1088/1361-648x/aaf74b

Peer reviewed

Effect of wavefunction delocalization on shift current generation

Liang Z. Tan[1] and Andrew M. Rappe[2]

[1]*Molecular Foundry, Lawrence Berkeley National Laboratory, Berkeley, California 94720, United States*

[2]*Department of Chemistry, University of Pennsylvania, Philadelphia, PA 19104, United States of America*

Abstract

We derive upper bounds on the magnitude of shift photocurrent generation of materials in two limiting cases: the flat-band limit of almost-isolated systems such as molecular crystals, and the wide-band limit of one-dimensional or quasi-one-dimensional materials such as ferroelectric polymers or other materials with chain-like motifs. These bounds relate the magnitudes of the shift current bulk photovoltaic effect to materials parameters. In both cases, we find that ratio of electron hopping amplitudes to the band gap plays a vital role in maximizing the amount of nonlinear response. Furthermore, by using the Wannier function formalism, we quantify the effect of long-range hopping amplitudes, showing how delocalization of electronic states gives rise to larger photocurrents. These results inform the design and selection of new materials for large shift current generation.

I. INTRODUCTION

Shift current is a leading candidate for the bulk photovoltaic effect, which is the generation of a photocurrent in the bulk of a noncentrosymmetric crystalline material, without the presence of interfaces [1]. Shift current is a nonlinear optical effect, and is driven by the coherent evolution of excited carrier wavefunctions under external illumination. The breaking of centrosymmetry is essential for shift current, as it provides preferred directions for current propagation. First studied in ferroelectrics [2, 3], the shift current has more recently been studied in topological and 2D materials [4–7], and proposed as means to achieve high efficiency light harvesting [8]. While there have been a number of other mechanisms proposed for the bulk photovoltaic effect [9–11], first-principles calculations and experiments indicate that shift current is expected to be a sizable contribution [12, 13]. As such, it is vital to assess the magnitudes of shift current not only for individual materials, but also to understand its trends across entire materials classes.

The delocalization of conduction and valence band wavefunctions has been suggested as an important parameter controlling the shift current magnitude [14]. Intuitively, the delocalization of the wavefunctions across different sites in a material favors the propagation of carriers when excited into these bands. These characteristics tend to be found in covalently bonded materials, and may be quantified by the tight-binding hopping amplitudes between orbitals located at the different sites of the material. It has been shown that, for a 3D bulk material, these hopping amplitudes, together with other materials parameters such as the band gap, place an upper bound on the maximum shift current attainable [15].

In this paper, we extend the analysis of Ref. [15] to one-dimensional materials, finding tighter bounds in two limiting cases: (i) where there are hopping amplitudes that are weak, and (ii) where there are hopping amplitudes that are strong. These findings are significant in the light of recent theoretical calculations of 1D systems and quasi-1D systems [14, 16] with the highest shift current responses predicted to date.

II. THEORY

Shift current can be derived from perturbation theory at second-order in the electric field strength of the light field [17]. Under illumination at frequency ω, the Cartesian components

of the photocurrent, J_r can be expressed in terms of the nonlinear conductivity σ_{rst} and Cartesian components of the electric field (E_s). It can be written as (summing over repeated indices)

$$\begin{aligned} J_r =& \sigma_{rst}(\omega) E_s E_t \\ \sigma_{rst}(\omega) =& \pi e \left(\frac{e}{m\hbar\omega}\right)^2 \sum_{cvk} \langle c|p_r|v\rangle\langle v|p_s|c\rangle \delta(\omega_c - \omega_v - \omega) \mathcal{R}_{rt}(c,v,k) \end{aligned} \tag{1}$$

which sums contributions, between every conduction (c) and valence (v) band pair and at every point in the Brillouin zone (k), of the transition dipole moments ($\langle c|p_r|v\rangle$ are matrix elements of the Cartesian components of the momentum operator, p_r) and the shift vector ($\mathcal{R}_{rt}(c,v,k)$). This photocurrent is generated only for transitions where the difference between conduction band ($\hbar\omega_c$) and valence band ($\hbar\omega_v$) energies is resonant with the incident light, as enforced by the δ-function in Eq. 1. The shift vector is a quantity that measures the change in the center of charge as it is excited from valence to conduction bands:

$$\mathcal{R}_{rt}(c,v,k) = -\frac{\partial}{\partial k_t} \arg\langle c|p_r|v\rangle - [\chi_{vt}(k) - \chi_{ct}(k)] \tag{2}$$

Here, it is given in terms of Berry connections of the conduction ($\chi_{ct}(k)$) and valence bands ($\chi_{vt}(k)$). This link between topological quantities and nonlinear optics has been explored in recent theoretical papers [4, 5, 18]. This formalism for calculating the shift current has been used in a number of first-principles simulations, which have been used to explain experimental observations of the bulk photovoltaic effect, and to predict new materials with large shift current responses [8].

The derivation of an upper limit on the shift current begins with the Wannierization of energy bands [19]. For simplicity, we consider the lowest conduction band and the highest valence band as these account for most of the optical response in solar-relevant applications. Unitary rotations of the Bloch functions in the space of these two bands results in maximally localized Wannier functions, and a tight-binding Hamiltonian for these two bands, which reproduces their band dispersion, and can be written as

$$H(\vec{k}) = \vec{h}(\vec{k}) \cdot \vec{\tau} = \sum_{i=1}^{3} h_i(\vec{k}) \tau_i \tag{3}$$

Here, the τ_i are Pauli matrices in the basis of the maximally localized Wannier functions for these two bands, and $\vec{h}(\vec{k})$ is a vector of 3 real parameters that parameterize this Hamil-

tonian. The approach taken here is equivalent to the diagonal tight-binding approximation of Ref. [20]. Being maximally localized, the hopping amplitudes between these Wannier functions would decay exponentially with their separation. They can therefore be bounded as

$$\begin{aligned} \vec{h}(\vec{k}) &= \sum_{n_1 n_2 n_3} \vec{h}_{n_1 n_2 n_3} \exp\left(i\vec{k}\cdot(n_1\vec{R}_1 + n_2\vec{R}_2 + n_3\vec{R}_3)\right) \\ |\vec{h}_{n_1 n_2 n_3}| &< A \exp\left(-\frac{n_1}{\xi_1} - \frac{n_2}{\xi_2} - \frac{n_3}{\xi_3}\right) \end{aligned} \tag{4}$$

for a 3D material. Here, $\vec{R}_j$ are the lattice vectors, and $\vec{h}_{n_1 n_2 n_3}$ are the hopping amplitudes between Wannier functions with relative displacement (n_1, n_2, n_3), and which decay with characteristic ranges (ξ_1, ξ_2, ξ_3). The quantity A is the upper bound for magnitude of the hopping amplitudes.

In Ref. [15], $M = \left|\hbar \int_{CB1,VB1} \sigma_{rrr} d\omega\right|$ was used as a figure of merit for the magnitude of shift current. This integral is taken over the energy range spanned by all transitions from the highest valence band (VB1) to the lowest conduction band (CB1), and gives an indication of the typical shift current magnitude in this energy range, for the longitudinal part of the response tensor, where the light polarization and current directions are parallel. This figure of merit can be written as

$$M = \frac{\pi e^3}{2\hbar} \left| \int \frac{d^3k}{(2\pi)^3} \frac{\vec{h}(\vec{k}) \cdot \vec{h}'(\vec{k}) \times \vec{h}''(\vec{k})}{E(\vec{k})^3} \right| \tag{5}$$

where the derivatives $\vec{h}' = \frac{d}{dk_r}\vec{h}$, $\vec{h}'' = \frac{d^2}{dk_r^2}\vec{h}$ are along the direction of light polarization and current, r. Here, $E(\vec{k})$ is the energy difference between conduction and valence bands at $\vec{k}$. A derivation of Eq. 5 is given in the Appendix. By using the bound on the hopping amplitudes (Eq. 4) in the evaluation of the shift current generated by the Hamiltonian Eq. 3, a general bound for the shift current of 3D materials was obtained Ref. [15].

$$M < \frac{2\pi e^3}{\hbar} \left(\frac{A}{E_g}\right)^2 \Xi\left(\vec{R}_1, \vec{R}_2, \vec{R}_3, \vec{\xi}, \hat{v}\right) \tag{6}$$

Here, E_g is the band gap, and $\vec{v}$ is a unit vector in the direction of light polarization and current measurement. Ξ is a rapidly growing function in $\vec{\xi}$, and quantifies the dependence of the shift current magnitude on wavefunction delocalization.

A. Derivation of bound in the flat-band limit

We now consider the behavior of the bound in some limiting cases, to better understand the effects of localization and hopping. Eq. 6 shows that wide band systems, which must necessarily have large A values, have the potential to have large responses. The limit of isolated systems (clusters or molecules), however, is not directly addressed by Eq. 6 because such systems can have large or small A values depending on the strength of the hopping within the isolated system. Nevertheless, a different upper bound can be derived for the nonlinear response of a system in the isolated, or flat-band limit.

To access this limit, we start with a one-dimensional system containing periodic images of an isolated system. We pass to the flat-band limit by letting the hopping between different images (λ) go to zero while keeping the hopping within the system fixed (Fig. 1). We assume that the Wannier centers of this system are separated by distance a. The effective Hamiltonian of this system takes a simple form, for there is only nearest-neighbor hopping between the two Wannier centers of this system in this limit.

$$H(k) = \lim_{\lambda \to 0} \begin{pmatrix} h_z & h_{xy}e^{-ika} + \lambda e^{-ik(L-a)} \\ h_{xy}e^{ika} + \lambda e^{ik(L-a)} & -h_z \end{pmatrix} \tag{7}$$

with k being the crystal momentum and L the size of the supercell. Here, $h_{xy} = \sqrt{h_x^2 + h_y^2}$ is the hopping between the two Wannier centers. In the limit $\lambda \to 0$, the Hamiltonian approaches $\vec{h}(k) = (h_{xy}\cos ka, h_{xy}\sin ka, h_z)$. To visualize the parameter space available for this system, we plot the graph of $\vec{h}$ as a function of k in Fig. 1, which shows that it is an arc with a radius the size of the hopping amplitude h_{xy}, and a height of the on-site potential difference h_z between the two Wannier centers. If the band gap E_g of this system is considered fixed, this arc is constrained to lie on a sphere of radius $E_g = 2\sqrt{h_{xy}^2 + h_z^2}$. For the Hamiltonian in Eq. 7, Eq. 5 gives

$$M = \frac{\pi e^3}{2\hbar}\frac{a^3}{V}\frac{h_{xy}^2 h_z}{(h_{xy}^2 + h_z^2)^{3/2}} \tag{8}$$

where V is the volume of the supercell. To bound the nonlinear response in this limit, we maximize Eq. 8 subject to the constraint that $E_g = 2\sqrt{h_{xy}^2 + h_z^2}$, i.e. with the height h_z of the arcs in Fig. 1 as the only independent degree of freedom. We note from Eq. 8 that the extreme cases of $h_z = 0$ and $h_z = E_g/2$ both give no nonlinear response. The former case is

centrosymmetric as both Wannier centers have the same on-site energy, while the latter has vanishing oscillator strength for the transition between two Wannier centers.

We find that the optimal value is $h_z = E_g/(2\sqrt{3})$. To rewrite this in terms of the oscillator strengths, we use $f_{cv} = \frac{2m\omega_{cv}}{\hbar}|r_{cv}|^2$, and

$$|r_{cv}|^2 = \frac{(h_z \frac{d|h|}{dk} - |h|\frac{dh_z}{dk})^2 + (h_x \frac{dh_y}{d_k} - h_y \frac{dh_x}{d_k})^2}{4|h|^2(|h|^2 - h_z^2)} \tag{9}$$

as derived in [21]. At the optimum point, we have $|r_{cv}|^2 = a^2/6$, which results in

$$M < \frac{\pi e^3}{\hbar} n \left(\frac{\hbar^2 f_{cv}}{m E_g}\right)^{3/2} \tag{10}$$

where $n = 1/V$ is the number density of molecules and f_{cv} the oscillator strength of the HOMO-LUMO transition.

Second harmonic generation (SHG) is another nonlinear optical phenomenon closely related to shift current generation. While both are second-order nonlinearities, SHG results in an response at frequency 2ω, whereas shift current results in a zero-frequency response (dc current). The expressions for the susceptibilities of both processes are very similar [17, 22, 23], which suggests that materials that have large shift currents would have large SHG susceptibilities as well. However, there are some differences between this and earlier work on the limits of SHG [24, 25]. We emphasize that the formalism [17] used here only considers the resonant component of the nonlinear response. In this respect, Eq. 10 is different from the off-resonant SHG bound for molecules proved by Kuzyk [24], in which the frequency of light is not resonant with any electronic transitions. In using Eq. 1, we are implicitly assuming that broadening of bands caused by phonons, disorder, or many-body effects is less than the band width. In this limit, the amount of broadening (width of δ-functions) in Eq. 1 is inconsequential as it does not affect the energy integral in $M = |\int \sigma dE|$. In contrast, the expressions for resonant molecular SHG in Ref. [25] depend on a broadening parameter because they are applicable in the limit where broadening is larger than the band width. Therefore, the bound Eq. 10 proved here should be interpreted as the maximum response of almost isolated systems, as the hopping between images tends towards zero.

The total steady-state photocurrent of a completely isolated system consists of multiple components, including the shift current and recombination current, which must all sum to

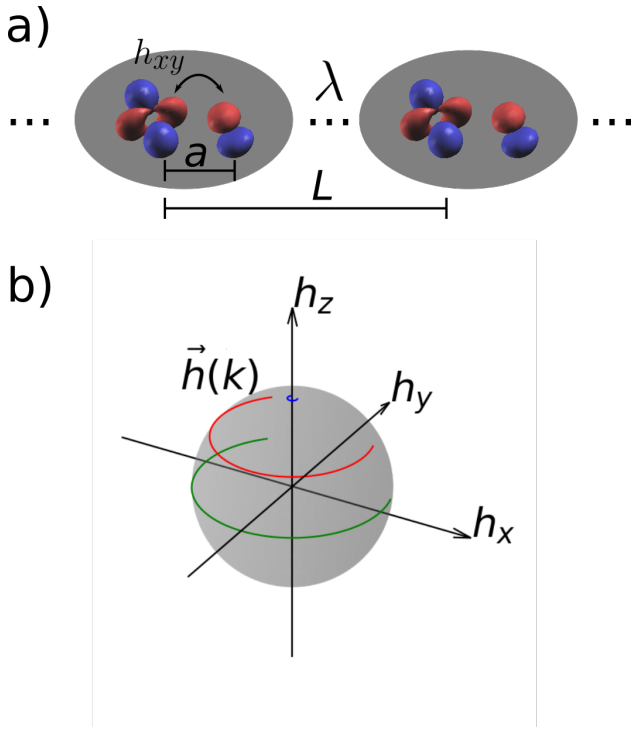

FIG. 1. a) Schematic of one-dimensional system in the isolated, or flat-band limit. The hopping amplitude between periodic images of the system (λ) vanishes, while the hopping amplitude between the Wannier centers within the system (h_{xy}) is kept finite. The Wannier centers have relative displacement a in a supercell of size L. b) Graph of the Hamiltonian parameters of isolated systems. At each point in the Brillouin zone, k, the parameters $\vec{h}(k) = (h_x, h_y, h_z)$ together define the Hamiltonian $H(k)$ via Eqs. 3 and 7. The path that $\vec{h}(k)$ takes through parameter space as k traverses the Brillouin zone is plotted as a continuous line, with endpoints corresponding to $k = -\pi/L$ and $k = \pi/L$. The constant energy splitting between HOMO and LUMO constrains $\vec{h}(k)$ to lie on a sphere (shaded gray). Shown in color are an inversion symmetric case ($h_z = 0$, green), the optimal case that maximizes the nonlinear response (red), and a case with vanishing oscillator strength ($h_{xy} = 0$, blue). For each case, the contributions to the nonlinear response is constant for all wavevectors k.

zero. While the shift current is argued [1, 12, 26] to be the dominant component in extended systems, it is cancelled by the recombination current if open-circuit conditions are strictly enforced. We emphasize that the above bound only applies to the shift current component of the current in this limit.

B. Derivation of bound in the wide-band limit

Next, we consider the limit of strong hopping. We consider a one-dimensional system where the hopping parameters are allowed to increase while keeping the band gap fixed at E_g. In contrast to the previous section where the energy bands were flat, the case considered here corresponds to the wide-band limit. Again, the Hamiltonian is defined by $\vec{h}(k)$, which we plot as a path in parameter space in Fig. 2a. As we pass from the flat-band limit to the wide band limit, the graph of $\vec{h}(k)$ changes from a circular arc of radius $E_g/2$ (Fig. 1) to a path with $\min_k|\vec{h}(k)| = E_g/2$. The length of this path increases as the hopping strength increases. As this happens, the majority of the nonlinear response is concentrated near the band edges (light colored regions in Fig. 2). In addition, the magnitude of $\vec{h}''(k)$ near the band edge increases, which increases the total amount of nonlinear response, as allude. We now show that these features are generically present for one-dimensional systems, under the assumptions of finite range hopping and nondegenerate band minima.

We start with some arbitrary fixed Hamiltonian with parameters $\vec{h}_{\text{fix}}(k)$ and add an adjustable correction which scales the hopping magnitude, so that the parameters of $H(k)$ are

$$\vec{h}(k) = \vec{h}_{\text{fix}}(k) + \lambda\vec{\Delta}(k) \tag{11}$$

We are interested here in the strong hopping limit of large λ. The exact choice of $\vec{h}_{\text{fix}}(k)$ does not matter as we approach this limit as its contribution will eventually become negligible. We assume that the Fourier components are exponentially bounded, as in Eq. 4:

$$\begin{aligned} |\vec{h}_{\text{fix},n}| &< A_{\text{fix}}e^{-n/\xi} \\ |\vec{h}_n| &< Ae^{-n/\xi} \end{aligned} \tag{12}$$

where $\vec{h}_{\text{fix}}(k) = \sum_n \vec{h}_{\text{fix},n}e^{inkL}$, $\vec{h}(k) = \sum_n \vec{h}_n e^{inkL}$, and $\vec{\Delta}(k) = \sum_n \vec{\Delta}_n e^{inkL}$. By the triangle inequality, these two bounds limit the magnitude and the distance (n) dependence of the adjustable part of the Hamiltonian

$$\begin{aligned} \lambda|\vec{\Delta}_n| &< Ae^{-n/\xi} + A_{\text{fix}}e^{-n/\xi} \\ &< 2Ae^{-n/\xi} \end{aligned} \tag{13}$$

where we have used $A > A_{\text{fix}}$ since we are interested in the limit $A \to \infty$.

Furthermore, we assume that the adjustable part of the Hamiltonian does not change the band gap of the system: $\vec{\Delta}(k = 0) = 0$ because we wish to fix the band gap to be constant

in order to investigate how it affects the final expression for the figure of merit. We assume that the band gap occurs at only a single point in the Brillouin zone. Here, the band gap location is taken to be at $k = 0$ without loss of generality. Apart from these conditions, the form of $\vec{\Delta}(k)$ is otherwise not constrained.

We write the figure of merit for the integrated nonlinear response as (Eq. 5)

$$M = \frac{\pi e^3}{2\hbar} n_1 \left| \int \frac{dk}{2\pi} \frac{\hat{h}(k) \cdot (\vec{h}'_{\text{fix}}(k) + \lambda \vec{\Delta}'(k)) \times (\vec{h}''_{\text{fix}}(k) + \lambda \vec{\Delta}''(k))}{|\vec{h}_{\text{fix}}(k) + \lambda \vec{\Delta}(k)|^2} \right| \tag{14}$$

where n_1 is the areal density of these one-dimensional systems. Performing a Taylor expansion about $k = 0$,

$$\begin{aligned} \vec{h}_{\text{fix}}(k) &= \vec{h}_{\text{fix}}(0) + \vec{h}'_{\text{fix}}(0)k + \frac{1}{2}\vec{h}''_{\text{fix}}(0)k^2 \\ \vec{\Delta}(k) &= \vec{\Delta}'(0)k + \frac{1}{2}\vec{\Delta}''(0)k^2 \end{aligned} \tag{15}$$

we see that the factor $1/|h|^2$ approaches a δ-function as $\lambda \to \infty$

$$\begin{aligned} \lim_{\lambda\to\infty} \frac{1}{|\vec{h}_{\text{fix}}(k) + \lambda\vec{\Delta}(k)|^2} &= \lim_{\lambda\to\infty} \frac{1}{|\vec{h}_{\text{fix}}(0)|^2 + (\lambda\vec{\Delta}'(0))^2 k^2} \\ &= \frac{\pi}{\lambda E_g |\vec{\Delta}'(0)|} \delta(k) \end{aligned} \tag{16}$$

This δ-function signifies that the contribution to the shift current is concentrated near the band edge in the wide-band limit. As $\lambda \to \infty$, we discard the terms in the numerator of Eq. 14 which are proportional to λ^0 and λ^1 in favor of the larger $\lambda^2 \hat{h} \cdot \vec{\Delta}' \times \vec{\Delta}''$, which yields

$$M < \frac{\pi e^3}{2\hbar} n_1 \frac{\lambda |\vec{\Delta}''(0)|}{2E_g} \tag{17}$$

The second derivative $\lambda|\vec{\Delta}''(0)|$ is bounded by

$$\begin{aligned} \lambda|\vec{\Delta}''(0)| &< \sum_n n^2 L^2 \lambda |\vec{\Delta}_n| \\ &< 2A \sum_n n^2 L^2 e^{-n/\xi} \end{aligned} \tag{18}$$

Where we have used the bounds of the distance (n) dependence of $\vec{\Delta}_n$ (Eq. 17). Combining Eqs. 17 and 18, we find that the figure of merit for total nonlinear response follows the asymptotic bound

$$M < \frac{\pi e^3}{\hbar}\frac{A}{E_g}\Xi_1(\xi) \tag{19}$$

as $A/E_g \to \infty$, where $\Xi_1(\xi) = 2n_1L^2\frac{e^{-1/\xi}+e^{-2/\xi}}{(1-e^{-1/\xi})^3}$. This bound, being proportional to A/E_g, is tighter than the general bound ($(A/E_g)^2$, Eq. 6) in the wide-band limit (large A/E_g). The reason for the different power law in the one-dimensional wide-band limit can be deduced from Eq. 5. While $\vec{h}'(k)$ and $\vec{h}''(k)$ are both proportional to A in magnitude, the region of the Brillouin zone which contributes to the nonlinear response is inversely proportional to A, leading to the overall linear in A scaling of Eq. 19.

Finally, we discuss the special case where the adjustable part of the Hamiltonian is stationary at $k = 0$: $\vec{\Delta}'(0) = 0$. This corresponds to the choice of not changing the Hamiltonian at $k = 0$. This should not be expected to result in a larger figure of merit than if one is allowed to change the Hamiltonian at $k = 0$. Even though Eq. 16 diverges when $\vec{\Delta}'(0) = 0$, the bound is not affected. Eq. 16 becomes

$$\begin{aligned}\lim_{\lambda\to\infty}\frac{1}{|\vec{h}_{\text{fix}}(k)+\lambda\vec{\Delta}(k)|^2} &= \lim_{\lambda\to\infty}\frac{1}{|\vec{h}_{\text{fix}}(0)|^2+(\lambda\vec{\Delta}''(0)\cdot\vec{h}_{\text{fix}}(0))k^2} \\ &= \frac{\pi}{E_g\sqrt{\lambda|\vec{\Delta}''(0)\cdot\vec{h}_{\text{fix}}(0)|}}\delta(k)\end{aligned} \tag{20}$$

while the numerator of Eq. 14 scales as $\hat{h}(k)\cdot\vec{h}'_{\text{fix}}(k)\times\lambda\vec{\Delta}''(k)$, leading to an overall scaling of $\sqrt{\lambda}$, which is of subleading order compared to Eq. 17.

III. CONCLUDING REMARKS

In summary, we have found upper bounds of the shift current response in two limits: the flat-band limit corresponding to almost-isolated systems, and the wide-band limit of extended 1D systems corresponding to strong hopping and electron delocalization. A common trend emerges from the analysis of these limiting cases. In both cases, the upper bound is increased by having a small band gap and a large hopping strength (oscillator strength, for the flat-band limit) between the Wannier centers of the system. These features are also shared by the general bound for 3D materials, although with a different scaling behavior. The bound for the wide-band limit contains an additional factor not present in the flat-band limit; $\Xi_1(\xi)$ describes the enhancement of shift current with the hopping range ξ(i.e.

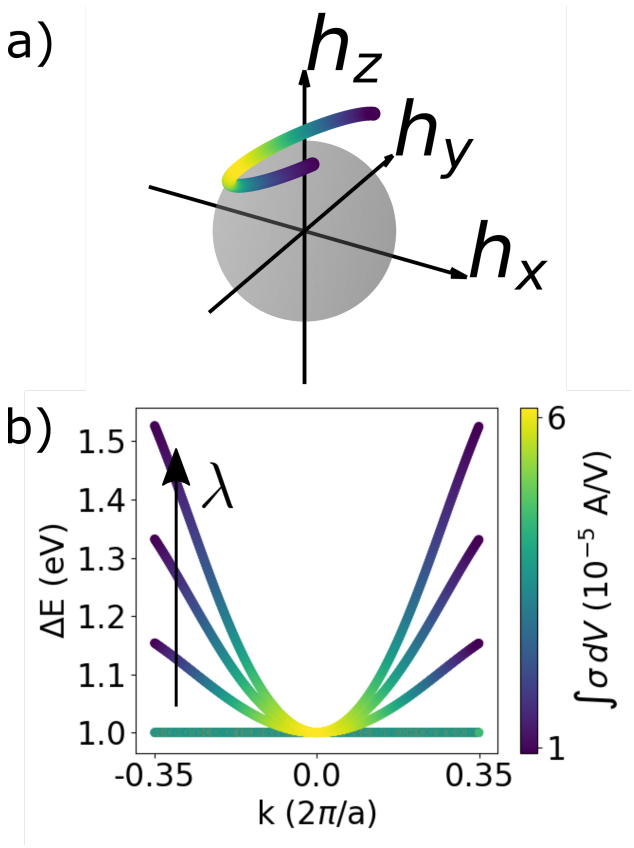

FIG. 2. a) Graph of the Hamiltonian parameters of an extended system. At each point in the Brillouin zone, k, the parameters $\vec{h}(k) = (h_x, h_y, h_z)$ together define the Hamiltonian $H(k)$ via Eqs. 3 and 11. The path that $\vec{h}(k)$ takes through parameter space as k traverses the Brillouin zone is plotted as a continuous line, with endpoints corresponding to $k = -\pi/L$ and $k = \pi/L$. I this plot, the energy difference between conduction and valence bands is given by the distance from the origin. The band gap is located at the intersection with the constant energy surface of radius $E_g/2$ (sphere shaded gray). The contribution to the nonlinear response is depicted in color, with the regions near the band gap having large (light color) contributions, and the regions away from the band gap having low (dark color) contributions. b) Band structure plot of a sequence of 1d Hamiltonians, given by Eqs. 3 and 11, showing the evolution from the flat-band limit to the wide-band limit as λ increases. As in a), the contribution to the nonlinear response is depicted in color. In the flat-band limit, moderate contributions are distributed evenly throughout the Brillouin zone, while the wide-band limit has large contributions predominantly at the band edges.

hopping beyond nearest-neighbors). We find that shift current is sensitive to the hopping range, asymptotically scaling as ξ^3 for very long range hopping, but not as sensitive as the 3D case, where the asymptotic scaling is ξ^9.

The bounds discussed here are valid only in their respective limits. On the other hand, they are tighter than the general bound for 3D materials in Ref. [15]. For the flat-band limit, we have explicitly constructed a model that saturates the bound. In the wide-band limit, the bound derived here is asymptotically smaller than the bound for 3D materials, in the limit of large hopping magnitudes. These bounds therefore afford a greater amount of certainty in suggesting materials design strategies for shift current materials.

To relate the results presented here to a specific material system, we consider the class of polar, conjugated polymers. A series of these have been recently predicted to support large shift currents [16]. The polymers constructed in this series contained two different heterocyclic rings, and varying numbers of vinylene linkage units, which result in the breaking of inversion symmetry necessary to support shift current. These polymers were computed to have large shift currents compared to other benchmark polar materials. An analysis of the band edge wavefunctions showed highly delocalized wavefunctions, which is in agreement with the general trend suggested by the upper bounds in this work. Furthermore, in Ref. [16], optimizing the magnitude of the current by changing the vinylene chain lengths showed that chains with smaller band gaps had larger shift currents, if the structures were otherwise the same. This observation is consistent with the inverse scaling with E_g shown above (Eq. 19). It should be stressed that these bounds should be interpreted as descriptors of aggregate behavior, and may not always reflect the effects of making structural modifications to any individual material, depending on the proximity of a material to the upper bound, and because such modifications may affect more than one of the factors which enter into the upper bounds.

We expect that these results will be useful in the selection and design of materials for novel photovoltaics. The flat-band limit is applicable to systems consisting of weakly interacting components, such as molecular crystals, while the wide-band limit is applicable to extended 1d systems. The latter includes the organic systems discussed above, which have experimental reports of large nonlinear response [27, 28]. The wide-band limit also includes bulk materials containing chain-like 1D motifs, such as some ternary alkali-metal chalcoarsenates [14, 29]. From the perspective of the wide-band limit, these materials seem

particularly attractive because of the combination of high packing density of 1D chains with strong extended hopping amplitudes along the chain direction.

IV. APPENDIX: DERIVATION OF EQ. 5

Here, we outline the derivation of Eq. 5, following Ref. [6]. We first rewrite Eq. 1 in terms of inter-band position matrix elements

$$r^a_{cv} = \langle c|i\frac{d}{dk_a}|v\rangle = |r^a_{cv}|e^{-i\phi^a_{cv}} \tag{21}$$

where we have introduced the phase of the position matrix elements, ϕ_{cv}. The k-space generalized derivatives of the position matrix elements are

$$\begin{aligned} r^a_{cv;b} =& \frac{d}{dk_b} r^a_{cv} - i(\chi_{cb} - \chi_{vb})\, r^a_{cv} \\ =& \left(\frac{d}{dk_b}|r^a_{cv}|\right)\, e^{-i\phi^a_{cv}} + |r^a_{cv}|\, e^{-i\phi^a_{cv}}\, \frac{d}{dk_b} e^{-i\phi^a_{cv}} - i(\chi_{cb} - \chi_{vb})\, r^a_{cv} \end{aligned} \tag{22}$$

Re-expressing the momentum matrix elements in terms of position matrix elements,

$$r^a_{cv} = \frac{\hbar\langle c|p_a|v\rangle}{i(\hbar\omega_c - \hbar\omega_v)m} \tag{23}$$

the equation for the nonlinear conductivity (Eq. 1) can be written as

$$\sigma_{aab} = \frac{\pi e^3}{\hbar^2} \sum_{cvk} \mathrm{Im}\left[r^a_{vc} r^a_{cv;b}\right] \delta(\omega_c - \omega_v - \omega) \tag{24}$$

This form of the conductivity is simpler for two-band systems when evaluated using a sum rule for $r^a_{cv;b}$. The general sum rule is (Ref. [6])

$$r^a_{cv;b} = -\frac{1}{\hbar\omega_c - \hbar\omega_v}(r^a_{cv}\Delta^b_{cv} + r^b_{cv}\Delta^a_{cv}) + \frac{w^{ab}_{cv}}{i(\hbar\omega_c - \hbar\omega_v)} + \sum_{p\neq c,v}\left(i r^a_{cp} r^b_{pm}\frac{\omega_{cp}}{\omega_{cv}} - i r^b_{cp} r^a_{pm}\frac{\omega_{pv}}{\omega_{cv}}\right) \tag{25}$$

Here, $w^{ab}_{cv} = \langle c|\frac{d^2}{dk_a dk_b}H|v\rangle$ and $\Delta^b_{cv} = \frac{d}{dk_b}(\hbar\omega_c - \hbar\omega_v)$. For two band systems, the last term in Eq. 25 vanishes. The first term in Eq. 25 does not contribute to $\mathrm{Im}\left[r^a_{cv} r^a_{cv;b}\right]$ in Eq. 24 when the light polarization direction is parallel to the current direction ($a = b$), which is the case treated here. The figure of merit becomes

$$M = \frac{2\pi e^3}{\hbar} \sum_k \left| \frac{\mathrm{Im}[r^a_{vc} w^{aa}_{cv}]}{\hbar\omega_c - \hbar\omega_v} \right| \tag{26}$$

Here, the sum over conduction and valence bands has been removed because we are treating a two-band system, but the factor of 2 arises from spin degeneracy. By writing $r^a_{cv} = -i\langle c|\frac{d^2}{dk_a}H|v\rangle/(\hbar\omega_c - \hbar\omega_v)$, we see that Hamiltonian derivatives are required for the evaluation of the figure of merit, Eq. 26. For a two-band system given by the Hamiltonian Eq. 3, the wavefunctions can be written explicitly

$$\begin{aligned} |c\rangle =& \frac{1}{\sqrt{2|h|}}(-\sqrt{|h| - h_z},\ e^{i \arctan(h_y/h_x)}\sqrt{|h| + h_z}) \\ |v\rangle =& \frac{1}{\sqrt{2|h|}}(\sqrt{|h| + h_z},\ e^{i \arctan(h_y/h_x)}\sqrt{|h| - h_z}) \end{aligned} \tag{27}$$

Using these wavefunctions in the evaluation of the Hamiltonian derivatives $\langle c|\frac{d^2}{dk_a}H|v\rangle$ and $\langle c|\frac{d^2}{dk_a dk_b}H|v\rangle$ in Eq. 26 results in the expression of the figure of merit in terms of the Hamiltonian parameters $\vec{h}$ and its derivatives $\vec{h}', \vec{h}''$ which is Eq. 5.

V. ACKNOWLEDGEMENTS

LZT acknowledges support from the Molecular Foundry at Lawrence Berkeley National Laboratory, supported by the Office of Science, Office of Basic Energy Sciences, of the US Department of Energy under contract No. DE-AC02-05CH11231. AMR acknowledges support from the US Department of Energy under grant DE-FG02-07ER46431. Computational support was provided by the NERSC of the US DOE.

[1] L. Z. Tan, F. Zheng, S. M. Young, F. Wang, S. Liu, and A. M. Rappe, npj Comp. Mater. **2**, 16026 (1 (2016).

[2] V. Fridkin, A. Grekov, P. Ionov, A. Rodin, E. Savchenko, and K. Mikhailina, Ferroelectrics **8**, 433 (1974).

[3] A. M. Glass, D. von der Linde, D. H. Auston, and T. J. Negran, J. Elec. Mat. **4**, 915 (1975).

[4] T. Morimoto and N. Nagaosa, Science Advances **2**, e1501524 (2016).

[5] L. Z. Tan and A. M. Rappe, Physical Review Letters **116**, 237402 (2016).

[6] A. M. Cook, B. M. Fregoso, F. d. Juan, S. Coh, and J. E. Moore, Nature Communications **8**, 14176 (2017).

[7] S. R. Panday and B. M. Fregoso, J. Phys.: Condens. Matter **29**, 43LT01 (2017).

[8] T. Rangel, B. M. Fregoso, B. S. Mendoza, T. Morimoto, J. E. Moore, and J. B. Neaton, Phys. Rev. Lett. **119**, 067402 (2017).

[9] V. Belinicher and B. Sturman, Soviet physics, Solid state. **20**, 476,481 (1978).

[10] E. Ivchenko, Y. B. Lyandageller, G. Pikus, and R. Y. Rasulov, Soviet physics,Semicoductors **18**, 55 (1984).

[11] V. I. Belinicher, Ferroelectrics **83**, 29 (1988).

[12] S. M. Young and A. M. Rappe, Phys. Rev. Lett. **109**, 116601 (2012).

[13] D. Daranciang, M. J. Highland, H. Wen, S. M. Young, N. C. Brandt, H. Y. Hwang, M. Vattilana, M. Nicoul, F. Quirin, J. Goodfellow, T. Qi, I. Grinberg, D. M. Fritz, M. Cammarata, D. Zhu, H. T. Lemke, D. A. Walko, E. M. Dufresne, Y. Li, J. Larsson, D. A. Reis, K. Sokolowski-Tinten, K. A. Nelson, A. M. Rappe, P. H. Fuoss, G. B. Stephenson, and A. M. Lindenberg, Phys. Rev. Lett. **108**, 087601 (2012).

[14] J. A. Brehm, S. M. Young, F. Zheng, and A. M. Rappe, The Journal of chemical physics **141**, 204704 (2014).

[15] L. Z. Tan and A. M. Rappe, arXiv:1708.05433 [cond-mat, physics:physics, physics:quant-ph] (2017), arXiv: 1708.05433.

[16] S. Liu, F. Zheng, and A. M. Rappe, J. Phys. Chem. C **121**, 6500 (2017).

[17] J. E. Sipe and A. I. Shkrebtii, Phys. Rev. B **61**, 5337 (2000).

[18] N. Nagaosa and T. Morimoto, Advanced Materials , 1603345 (2017).

[19] N. Marzari, A. A. Mostofi, J. R. Yates, I. Souza, and D. Vanderbilt, Rev. Mod. Phys. **84**, 1419 (2012).

[20] J. Ibañez-Azpiroz, S. S. Tsirkin, and I. Souza, Phys. Rev. B **97**, 245143 (2018).

[21] B. M. Fregoso, T. Morimoto, and J. E. Moore, Phys. Rev. B **96**, 075421 (2017).

[22] T. Morimoto and N. Nagaosa, Science Advances **2**, e1501524 (2016).

[23] L. Wu, S. Patankar, T. Morimoto, N. L. Nair, E. Thewalt, A. Little, J. G. Analytis, J. E. Moore, and J. Orenstein, Nat Phys **13**, 350 (2016).

[24] M. G. Kuzyk, Physical Review Letters **85**, 1218 (2000).

[25] M. G. Kuzyk, The Journal of Chemical Physics **125**, 154108 (2006).

[26] P. Král, J. Phys. Condens. Matter **12**, 4851 (2000).

[27] J. Pérez-Moreno, Y. Zhao, K. Clays, M. G. Kuzyk, Y. Shen, L. Qiu, J. Hao, and K. Guo, J. Am. Chem. Soc. **131**, 5084 (2009).

[28] M. Nakamura, S. Horiuchi, F. Kagawa, N. Ogawa, T. Kurumaji, Y. Tokura, and M. Kawasaki, Nature Communications **8**, 281 (2017).

[29] T. K. Bera, J. I. Jang, J.-H. Song, C. D. Malliakas, A. J. Freeman, J. B. Ketterson, and M. G. Kanatzidis, Journal of the American Chemical Society **132**, 3484 (2010).